4

High Performance DSSC using dimensionally controlled titania at sub-zero temperature, ZnO-TiO_2 and H-HfO_2/TiO_2 nanospheres as photoanode Materials

4.1 TITANIA AT SUB-ZERO TEMPERATURE (-40°C TO -10°C) AS PHOTOANODE MATERIAL

The TiO_2 nanocrystals (oval) and nanorods have several advantages due to their structural, optical and electrical properties. Nanorods were found to have more surface to volume ratio compared to nanocrystals. This would definitely have an impact on interfacial charge transfer rate. In nanorods, carriers are free to move along the length of the rods showing delocalization of charges and increase charge transport in DSSC. Whereas nanocrystals were exhibited high specific surface area, which is directly correlated to different size particle distribution along the photoanode films, also the roughness of the films have to be considered as a significant factor which directly influences the amount of dye loading.

4.1.1 Optimization of photoanode material

The DSSC with TiO_2 synthesized at subzero temperatures ranging from -40°C to -10°C were fabricated according to the process described in the Annexure A: Materials and methods. All fabricated DSSC have around 14 µm thick TiO_2 photoanode. The current density-voltage (J-V) characteristics are shown in Figure 4.1 and cells photovoltaic parameters were summarized in Table 4.1. The DSSC with photoanode materials as TiO_2 synthesized at -40°C and -10°C possess high efficiency among all the DSSCs, 3.3 and 3% respectively.

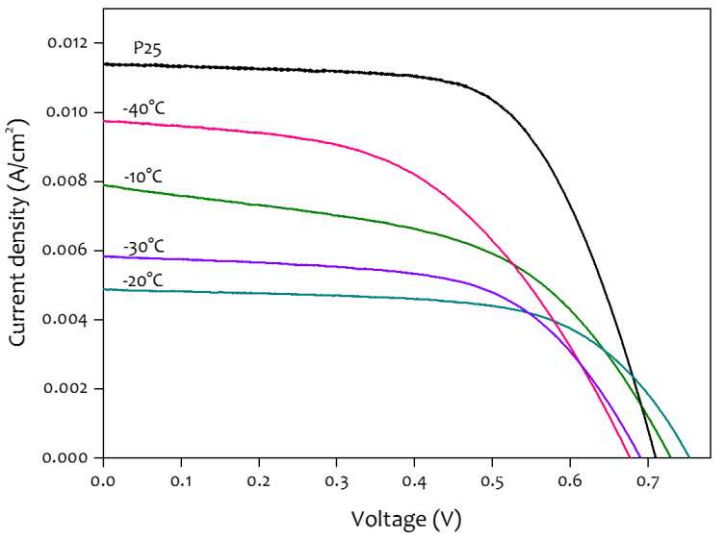

Figure 4.1 : Schematic illustration of nano-TiO_2 synthesis using reactor at temperatures ranging from -40°C to -10°C

Table 4.1: The current density-voltage (J-V) parameters of DSSC with different photoanode films

TiO_2 Synthesis temperatures (°C)	J_{sc} (mA/cm²)	V_{oc} (V)	FF (%)	η (%)
P25	11.4	0.71	64	5.2
-40	9.7	0.67	50	3.3
-30	5.5	0.67	57	2.1
-20	4.9	0.75	61	2.3
-10	7.9	0.73	50	3

Comparison of all J-V plots reveals that the main factor for enhancement in the efficiency of DSSCs is due to the phase and morphology of the TiO_2 nanoparticles. Also lower the band gap wider the range and more light will be absorbed by the wide band gap semiconductors. The DSSC with -40°C as photoanode consists of very small particle size, high specific surface area and anatase dominating TiO_2, and improves the performance of solar cells. As disused before at -10°C, particles were formed in nanorods shape and exhibited high weight percentage of the rutile phase, less lattice strain and low defects compare to other TiO_2.

The enhanced J_{sc} contributed to the increased light harvesting is related to the structural changes and dye loading. In DSSC the dye molecules are attached to the TiO_2 nanoparticles by forming ester bonds between carboxylic group present on the dye molecule and hydroxyl group from the TiO_2 surface. In certain cases, at -30°C and -20°C due to minimum surface free energy particle have high tendency to agglomerate and leads to cutting down of sites for dye loading to the TiO_2 surface and eventually hampers the light harvesting. There is direct impact of the subzero synthesis temperature on the TiO_2 structure along with its various properties, it also synergically effects the light harvesting in the DSSC.

If these samples will be used as photoanode in DSSC, wider band gap will reduce recombination in the DSSC allowing more electrons to jump from the excited state of the dye to the conduction band of TiO_2.

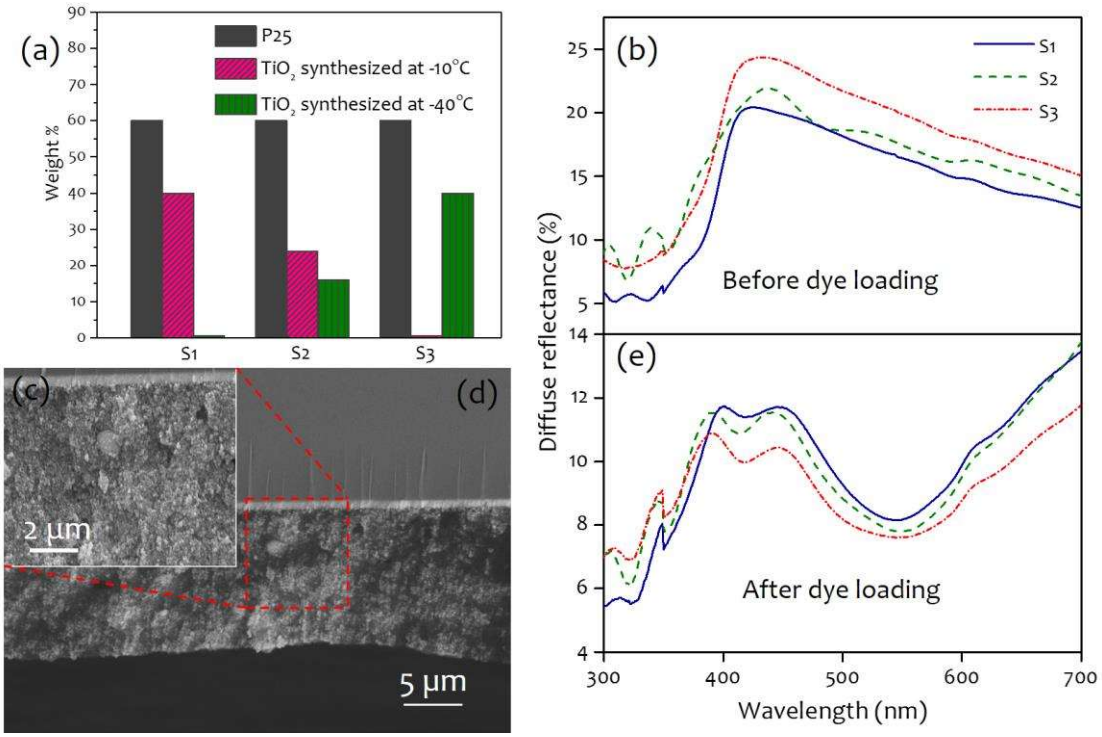

Figure 4.2 : (a) Bargraph shows the composition of S1, S2 and S3. (b) Cross sectional image of film S1 and inset SEM image show uniformly oriented nanoparticles with high porosity. (c) and (d) Diffuse reflectance spectra of S1, S2 and S3 photoanodes before and after dye loading respectively

To optimize DSSC performance, three samples S1, S2 and S3 were prepared with 0, 16 and 40 of wt % of TiO_2 prepared at -40°C in respective samples, the detailed composition is illustrated in the form of a bargraph in Figure 4.2a. The cross sectional film morphology was obtained by SEM (Figure 4.2d), the average thickness of the film was found to be 14.5 µm. The film thickness is optimized in the range of 10-18 µm range and its uniformity are the main parameters which control the reproducibility of the DSSC performance. Above this range, thickness produces resistance to electrons travelling through TiO_2 and also decreases the number of photons encountered by dye molecules. Below the optimized range number of anchoring site for dye molecules reduces. The inset of Figure 4.2d shows uniformly distributed samples along the photoanode films with a highly porous structure (Figure 4.2c).

4.1.2 Light scattering enhancement in photoanode films

The film surface morphology and the average root mean square roughness (R_{rms}) of S1, S2 and S3 samples are shown in the Figure 4.3, and are listed in Table 4.2. The films show columnar microstructure accompanied by spherical grain structure suggesting that it constitutes nanorods with oval shaped nanoparticles. As the concentration of TiO_2 synthesized at -40°C increases in sample S1 and S2 films, the intensity of the columnar microstructure was decreased as percentage of nanorods declined leading to reduced height of the columnar microstructure with increased size of spherical grains.

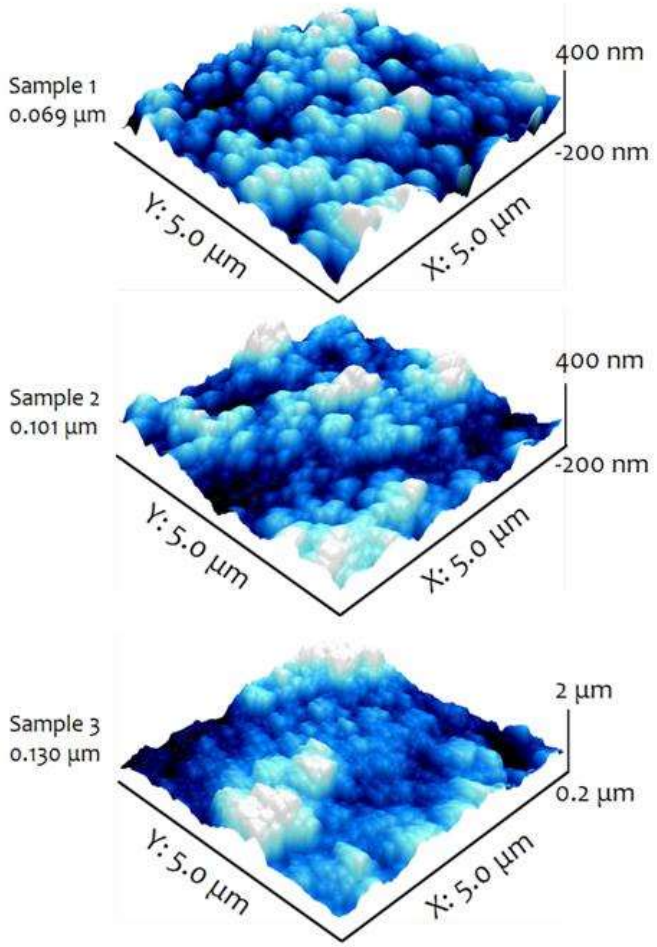

Figure 4.3 : AFM images of the S1, S2 and S3 sample photoanodes

At the highest concentration, an S3 film consisting of nanocrystals with bigger spherical grain size showed the lowest intensity in the columnar microstructure. The increased -40°C concentration in compositions enhances roughness along the films and clearly shows

improvement in the number of anchoring sites for the dye molecules and electrochemical property of the films.

Table 4.2: Different parameters of TiO_2 based photoanode films[a]

Samples	*wt% of TiO_2 prepared at -40 ℃ in sample*	*R_{rms} (mm)*	*Dye loading amount ($\times 10^{-9}$ mol cm^{-2})*
S1	0	0.069	3.6066
S2	16	0.101	3.9421
S3	40	0.130	4.2392

[a]These values refer to the percentage of the TiO_2 prepared at -40°C in sample and film surface root mean square roughness, R_{rms}

Light scattering property of photoanode films is one of the important attributers in light harvesting efficiency of the DSSC [Zhang, *et al.*, 2010; Shao, *et al.*, 2012]. The diffused reflectance of S3 film is higher as compared to the other photoanode films before dye loading as shown in Figure 4.2b. High percentage of anatase having different sized nanoparticles with higher surface roughness attributes to increased light scattering in S3 film and will harvest more light during photo conversion. After dye loading, diffused reflectance of all photoanode films were decreased significantly due to light absorption by the dye and are shown in Figure 4.2e. The dyed S3 photoanode film is reported to have more absorption with lower diffused reflectance in the 350-700 nm region compared to other samples.

The amount of dye loading at photoanodes directly have profound effect on the photocurrent density are summarized in Table 4.2 and Figure 4.4. The measured dye loading behavior matches with the trend of the UV-vis reflectance data. The specific surface area is directly correlated to different size particle distribution along the photoanode films, also the roughness of the films has to be considered as a significant factor which directly influences the amount of dye loading. This provides more number of sites to anchor dye molecules and shows S3 photoanode's dye loading capacity is higher compared to other samples (4.2392×10^{-9} mol/cm^2).

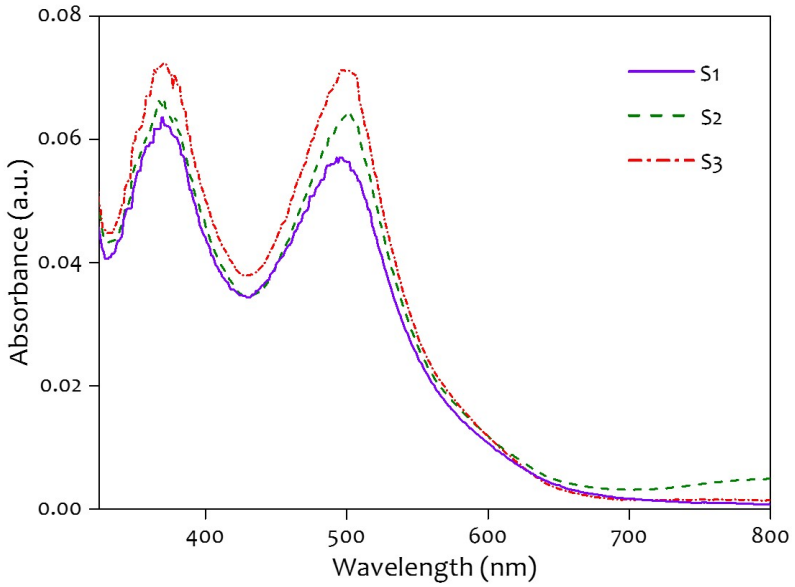

Figure 4.4 : Dye absorbed amount of S1, S2 and S3 sample photoanodes are calculated using absorption spectra

The size of TiO_2 prepared at -40°C was much smaller than that at -10°C. Smaller particles consists of large surface area and together with P25 particles photons from lights have more number of sites to scatter as shown in Figure 4.5.

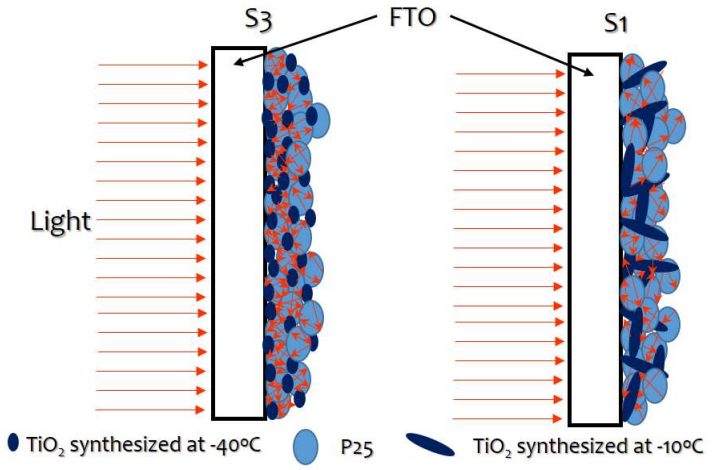

Figure 4.5 : Schematic showing film structures and their respective light scattering

4.1.3 Light harvesting, charge transport and recombination

The schematic diagram of DSSC is presented in Figure 4.6a and a photograph of one of the fabricated DSSC is shown in the inset of same.

Table 4.3: Parameters of DSSC fabricated at various conditions

Sample	Anatase Wt. %	Rutile Wt. %	*η (%)*
Anatase (ref. 46)	100	0	4.01
Rutile (ref. 47)	0	100	3.2
-40 oC	58	42	3.3
-10 oC	27	73	2.9

The current density-voltage curve and parameters of all DSSCs are reported in Figure 4.6b and Table 4.4 respectively. It has been observed that pristine P25, TiO_2 synthesized at -40°C or at -10°C were able to achieve 11.4 mA/cm² of photocurrent while S1, S2 and S3 combinations show remarkably higher photocurrent (see Table 4.3).

Table 4.4: Different parameters of DSSC with different photoanode films[a]

Sample	*Wt% of Anatase*	J_{sc} *(mA/cm²)*	V_{oc} *(V)*	*FF*	*η (%)*
-40°C	58	9.69±0.9	0.68±0.01	50.8±0.9	3.3±0.02
-10°C	27	7.86±0.02	0.73±0.01	50.79±0.2	2.9±0.05
P25	80	11.4±0.01	0.71±0.01	64±0.01	5.2±0.08
S1	59	17.44±1.4	0.68±0.01	57.67±0.33	6.9±0.5
S2	64	18.07±0.7	0.7±0.02	65.54±1.54	8.2±0.8
S3	71	18.46±0.4	0.7±0.01	66.46±1.46	8.6±0.3

[a]short circuit current density, J_{sc}, open circuit voltage, V_{oc}, fill factor, FF and photoconversion efficiency, η are the parameters of DSSC examined at AM 1.5G 1000 W/m² by keeping 0.09 cm² as the working area for all the solar cells

The S3 photoanode DSSC have high anatase percentage with oval shaped nanoparticles exhibiting high specific surface area with more sites to anchor more dye which eventually combines yielding enhanced photo-conversion efficiency and reported high efficiency of 8.6% compared to the other samples. Improving DSSC performance depends on the enhancement of the photocurrent J_{sc} which can be credited to the well-developed light scattering structure of the photoanode which increases the light harvesting, as the open circuit voltage V_{oc} and fill factor (FF) have little difference among the cells.

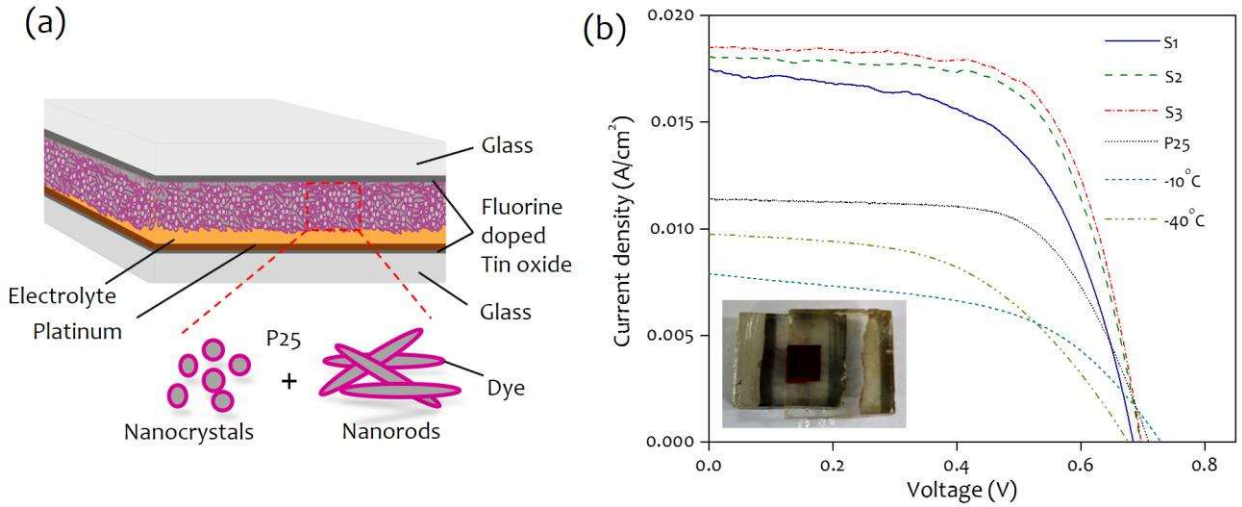

Figure 4.6 : (a) Schematic representation of fabricated DSSC. (b) Current density – voltage curves of the DSSC consisting -40 °C, -10 °C, P25, S1, S2 and S3 samples as photoanodes under one sun illumination

Reduced photocurrent in S2 and S3 can be explained by the less dye loading due to higher percentage of nanorods composition, low roughness and decreased sites to attach dye. Also, band gap of the TiO_2 prepared at -40°C is wider than -10°C, which exhibits faster electron transport at the interfaces [Yu, *et al.*, 2014]. It appears clearly from the above findings that efficiency is a function of percentage of the TiO_2 synthesized at -40°C in photoanodes, although particle size and shape also show their direct impact on the cell efficiency.

Electrochemical impedance spectroscopy (EIS) has been widely used to analyse various parameters attributed to electrons transport in the TiO_2 interface and recombination between electron at LUMO level of dye and the redox electrolyte are listed in the Table 4.5. Inset of Figure 4.7a shows the equivalent circuit of all fabricated DSSCs.

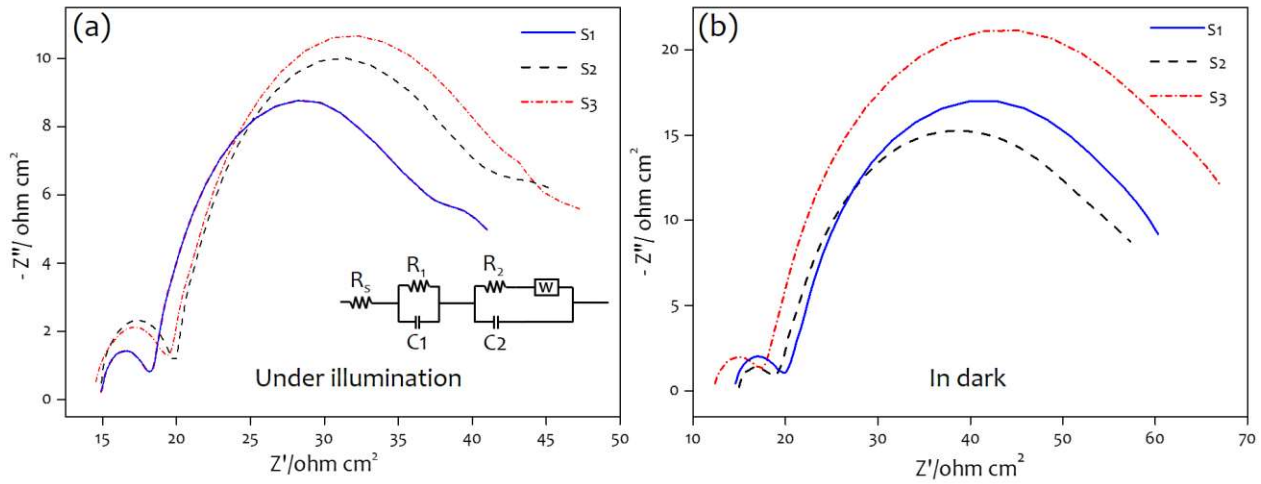

Figure 4.7 : Nyquist plot of DSSC with S1, S2 and S3 samples as photoanodes (a) under illumination and (b) in dark respectively

Under illumination, sheet resistance is observed as almost same for all DSSCs and as identical Pt counter electrodes were used during the fabrication, there is no significant change in the value of R_1. In such condition charge transport resistance R_2 decreased in S3 resulting in fast electron transport at electrolyte-dye-photoanode junction in the S3 DSSC shown in Figure 4.7a. In dark condition EIS shown in Figure 4.7b, no electron jumped from LUMO level of dye to TiO_2 and it implies transport of electrons to the electrolyte specimen. So R_2 transport resistance attributes recombination rate at these junctions [Zhang, *et al.*, 2013; Doh, *et al.*, 2004].

The sheet resistance (R_s) is the combine value of resistance of the FTO glass, contact resistance of the DSSC and resistance created due to external circuits.

Table 4.5: Experimental parameters of DSSC obtained by the equivalent circuit[b]

DSSC	*Under illumination*			*In dark*		
	R_s/Ω	R_1/Ω	R_2/Ω	R_s/Ω	R_1/Ω	R_2/Ω
S1	14.97	17.47	4.817	15.12	30.53	12.53
S2	14.82	19.11	4.63	15.45	26.73	3.757
S3	15.14	15.66	3.124	12.72	35.37	4.575

[b]Sheet resistance and series resistance are obtained under illumination at AM 1.5G 1000 W/m^2 and in dark. The derived parameters are corresponds to high performed cells in Table 4.4

The charge transfer between Pt counter electrode and electrolyte is demonstrated by first semicircle (R_1). The electron transfer at electrolyte-dye-photoanode interface serves as charge transport and recombination represented by the intermediate semicircle (R_2). Diffusion of the iodide species in electrolyte is shown by the third semicircle.

4.2 ZnO-TiO_2 HETEROJUNCTION SOLID NANOSPHERES AS PHOTOANODE

To understand the role of this heterojunction, dye sensitized solar cells (DSSC) is adopted as one of the simple and quick method. Attempts has been made towards exploring combination of TiO_2 and ZnO as photoanode materials in DSSC where explicit structural and morphology determines the photoconversion efficiency of cell [Pan, *et al.*, 2015; Zhang, *et al.*, 2011].

4.2.1 Nanosphere as electron trapping sites

The synthesis of a novel ZnO-TiO_2 heterojunction solid nanospheres decorated with different percentage of ZnO. The solid nanospheres are synthesized by an environmentally friendly and facile route.

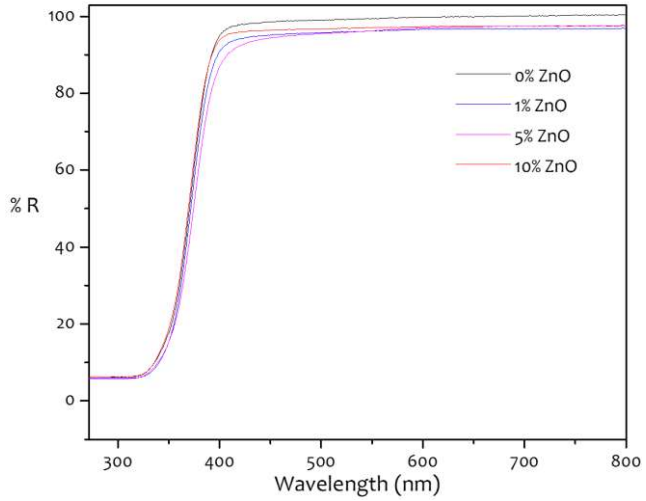

Figure 4.8 : UV-vis diffuse reflectance spectra of TiO_2 solid nanospheres with various ZnO %

These mesoporous structures are comprised of polydisperse aggregates of both oxides and possess type-II heterojunction. The ZnO-TiO_2 heterojunction architecture can separate the electrons and holes and provide more electron trapping sites. The high specific surface area solid nanospheres used as photoanode material in the DSSC can trap more light by facilitating higher number of sites for dye attachment. In addition, these heterojunctions have potential to

show increment in the electron trapping, as a result, charge recombination is suppressed and the performance of the DSSC is greatly enhanced.

The UV-vis diffuse reflectance spectra in the wide spectral range of 250-700 nm for TiO_2 solid nanospheres with different ZnO % are shown in Figure 4.8. The spectra show a decrease in reflectance upon increasing ZnO%. The decrease in reflectance is slightly higher ($\Delta R \sim 2\%$) for 1% doped ZnO as compared to 5% and 10% doped ZnO-TiO_2 samples resulting in enhancement in light scattering for 1% ZnO. The 1% ZnO/TiO_2 solid nanospheres scatter in visible light more efficiently as compared to the TiO_2 nanospheres alone since the average size is of the order of the wavelength of light. The densely packed solid nanospheres of both oxides can result in multiple scattering of light due to their random distribution [Wu, *et al.*, 2004; Cao, *et al.*, 2000].

4.2.2 Dye loading and light harvesting capability

The ZnO doped TiO_2 solid nanosphere films were used as photoanode layer in the dye-sensitized solar cell (DSSC) fabricated as detailed in the Annexure A: Materials and methods.

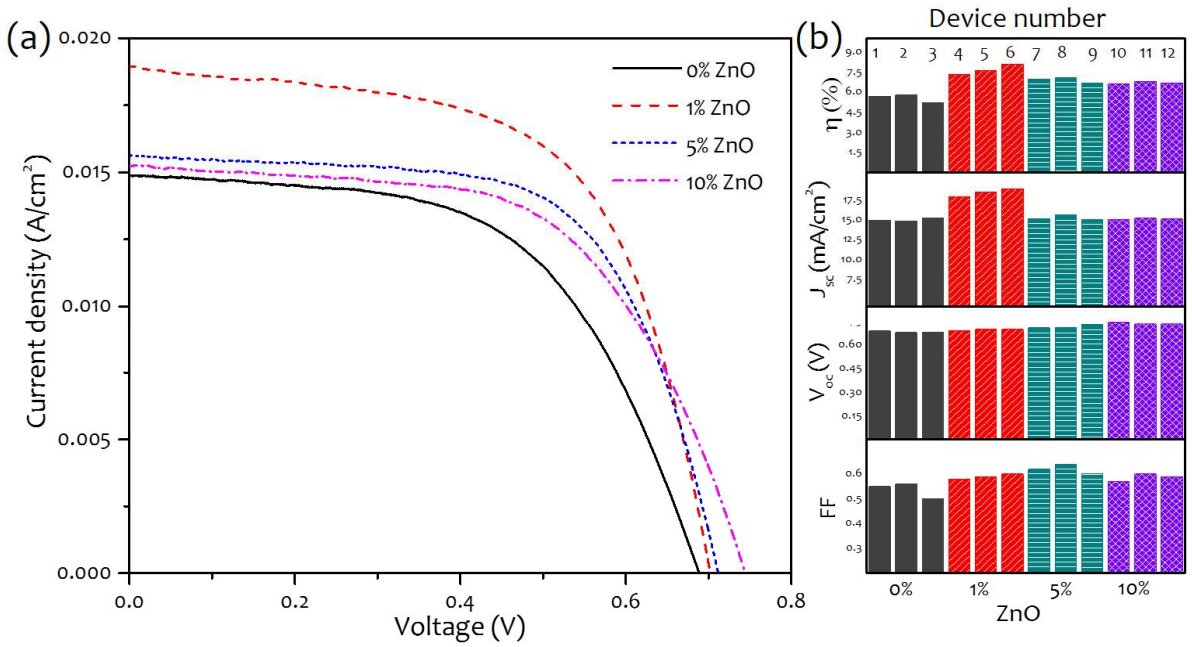

Figure 4.9 : (a) J-V characteristics of DSSC with photoanode based on TiO_2 solid nanospheres with different ZnO doping. (b) Bar graph displaying photovoltaic parameters obtained for different DSSC devices fabricated by varying the ZnO doping levels

The ZnO doped TiO_2 solid nanosphere material was screen printed in the form of a paste and annealed resulting in a photoanode with thickness of ~15 µm. The current density versus voltage (J-V) curves for DSSC devices fabricated using TiO_2 doped with ZnO of varying weight % are shown in Figure 4.9a.

Table 4.6: The photovoltaic properties of the dye sensitized solar cells based on ZnO doped TiO2 solid nanospheres[b]

ZnO %	*Average Pore Size (nm)*	*N_{719} Dye loading (nM cm²)*	*J_{sc} (mA/cm²)*	*V_{oc} (V)*	*FF*	*η (%)*
0	0.55	2.52	14.88	0.68	56	5.78
1	0.57	3.2	18.96	0.70	60	8.07
5	0.46	2.65	15.63	0.71	64	7.11
10	0.38	2.64	15.22	0.74	60	6.68

[b] J_{sc}, V_{oc}, FF and η are the short circuit photocurrent density, open circuit potential, fill factor and photo conversion efficiency respectively. The solar cell measurements were carried out under 1 Sun illumination

The performance parameters along with the dye loading amount on various photoanodes are summarized in Table 4.6. The effect of ZnO on the photovoltaic properties of TiO_2 can be quantitatively shown by the bar graph in Figure 4.9b. The 1% ZnO cell shows the highest J_{sc} up to 18.96 mA/cm² compared to 14.88, 15.63 and 15.22 mA/cm² for 0%, 5% and 10% doped cells. As the 1% showed maximum efficiency, we considered it important to examine the efficiencies of solar cells with ZnO between 1% and 5%. The 2% and 3% ZnO doped TiO_2 based DSSC exhibited J_{SC} of 17.73, and 16.22 mA/cm² respectively (see Figure 4.10) which is expected and in accordance with the trend as shown in Figure 4.9. The enhancement in photocurrent density for 1 % ZnO-TiO_2 based DSSC increases the overall efficiency.

Usually, the high photocurrent is an evidence of better dye loading. This predominantly increases the light harvesting capability of ZnO-TiO_2 based photoanode material [Wolf and Maret, 1985]. Dye loading capability of the photoanode was determined by the dye desorption using 10 mM NaOH solution, and the amount was calculated from the absorbance spectra shown in Figure 4.11.

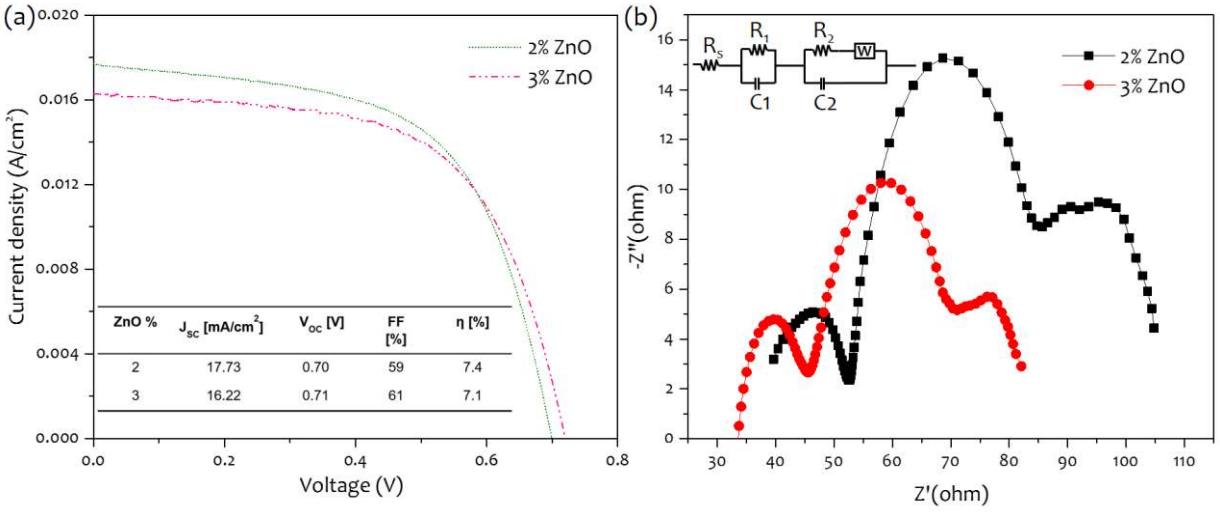

Figure 4.10 : (a) J-V characteristics and (b) Nyquist plot with equivalent circuit (inset) of ZnO-TiO_2 solid nanospheres with 2% and 3% ZnO as photoanode in DSSC

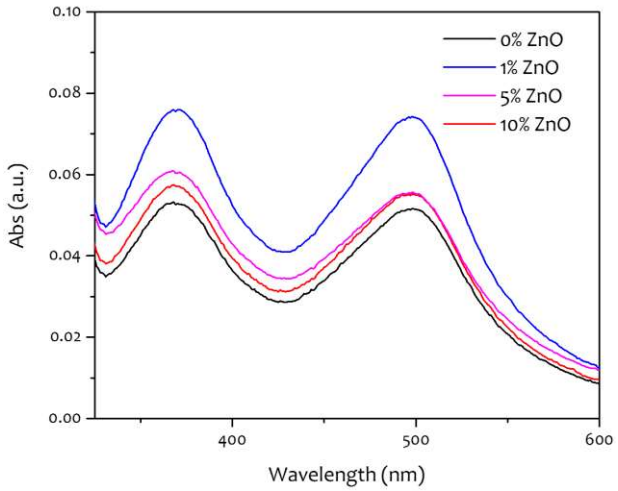

Figure 4.11 : Absorbance spectra of the TiO_2 solid nanospheres with various ZnO %. Amount of dye absorbed amount is calculated using Beers Lambert law

On ZnO doping, the increase in dye loading is lower (~21%) than the expected value based on efficiency ($\Delta\eta$ ~ 40%), however, the light harvesting capability is improved which improves the overall efficiency.

4.2.3 Electron transport and mobility

The electron transport in ZnO doped TiO_2 seems to be favorable as seen from the lower electrode resistance (Figure 4.12) and increase in the electron carrier density up to 47 % with increasing ZnO% (summarized in the Table 4.7). The charge resistance at their interface (R_{ct}) increases with increasing ZnO however the value for 1% ZnO is comparatively minimum (~13.88 Ω) as derived from the second semicircle and by fitting Nyquist plot with equivalent circuit as shown in Figure 4.12.

Table 4.7: The impedance study parameters of the ZnO doped TiO2 sphere dye sensitized solar cells[c]

ZnO doping %	f_{IMVS} *(Hz)*	τ_s *(ms)*	η_c *(%)*
0	14.2	0.045	40
1	10.8	0.039	42
5	12.6	0.028	44
10	12.8	0.034	47

[c] f_{IMVS} is the peak frequency in the Bode plots, τ_S electron lifetime and η_c charge collection efficiency

Since, the conduction band of ZnO formed by the s-orbital provides a significantly smaller μ_e (effective electron mass) compared to the higher μ_e corresponding to the d-orbital of TiO_2 conduction band, ZnO doped TiO_2 has more electron mobility than TiO_2. The enhancement in electron transport (~ 32%) as shown in Table 4.5 improves the photocurrent density, along with photovoltage and fill factor resulting in an increase in the photoconversion efficiency of the DSSC device. For ZnO % < 1, photocurrent density is relatively lower which can be attributed to the difference in crystallite size up to 10 nm and lower pore size of the nanosphere as shown in Table 4.6.

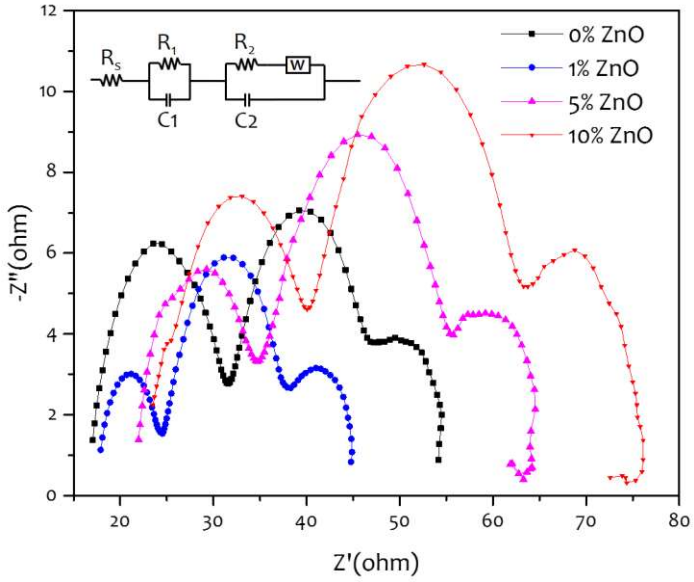

Figure 4.12 : Nyquist plot and equivalent circuit (inset) of ZnO-TiO_2 solid nanosphere with various ZnO % as photoanode in DSSC

This also reveals the reduced anchoring sites for N719 dye molecules further inhibits the photocurrent density in 5 and 10 % nanospheres. Although both photocurrent density and efficiency has deteriorated at higher doping percentage, open circuit voltage clearly shows enhancement up to 0.74 V (shown in figure 4.9b). The higher open circuit voltage is a result of less recombination rate at electrolyte interfaces. Both ZnO and TiO_2 exhibit similar band structures, as shown in the Figure 4.13. The incorporation of ZnO in TiO_2 makes energy at conduction band (E_{cb}) of ZnO more prominent, which easily transfer electrons to E_{cb} of TiO_2

rather than the electrolyte species [Li, *et al.*, 2015]. The path length is lowered at an optimized doping of 1% ZnO that further reduces the recombination rate at the electrolyte.

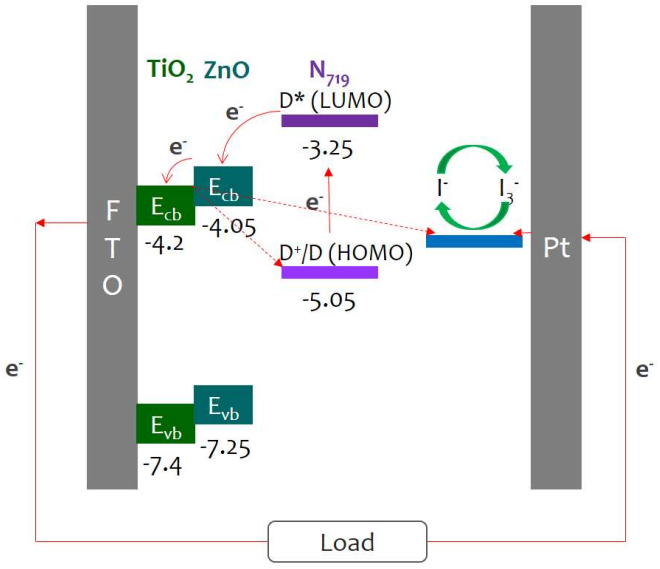

Figure 4.13 : Energy level diagram for working electrode of DSSCs based on TiO_2 solid nanosphere with various ZnO %

4.3 HYDROGENATED TiO_2 AND HfO_2 NANODOTS AS PHOTOANODE MATERIAL

The role of HfO_2 as a dopant in TiO_2 nanosphere have not been explored previously. The electronic shell of Hf in HfO_2 ($[Xe]4f^{14}5d^26s^2$) is loosely bound to the nucleus that can possibly contribute electrons to TiO_2 for improved conduction. Moreover, HfO_2 with high coordination sphere can offer high surface area and its dielectric nature can contribute towards enhanced optical absorption. Interestingly, the hydrogenation of HfO_2 is known to lower its resistance state, which can be utilized in synergy with hydrogenated TiO_2. Thus, TiO_2 with finely distributed HfO_2 nanodots is synthesized by combination of sol–gel and hydrothermal methods and hydrogenated. H-HfO_2/TiO_2 is compared with H-TiO_2 as a photoanode material and several devices have been fabricated. This emphasizes the feasibility of doping a high coordination sphere dielectric such as HfO_2 along with its hydrogenation, resulting in enhanced properties of TiO_2 photoactive material in all solar applications.

4.3.1 Hydrogenation, high surface area and light adsorption

The hydrogenated H-HfO_2/TiO_2 films were used as photoanode layer in the dye-sensitized solar cell (DSSC) fabricated as detailed in the Annexure A: Materials and methods. The cross-sectional view of the DSSCs fabricated using H-HfO_2/TiO_2 nanospheres is shown in Figure 4.14a. This represents the layer-by-layer arrangement of the photoanode to be used in the fabrication of DSSC. The magnified SEM image at the cross section is slightly uneven at the edge (Figure 4.14a; right); however, an in-depth focus shows the tightly packed morphology of the deposited film.

A schematic of the complete sandwich structure of DSSC is shown in Figure 4.14b. Figure 4.15a shows the J–V characteristics of the DSSC based on H-HfO_2/TiO_2, H-TiO_2 and P25 TiO_2. The corresponding photovoltaic parameters are detailed in Table 4.8. The H-HfO_2/TiO_2 photoanode based DSSC has a strikingly higher current density, J_{SC} of 21.74 mA/cm^2 with a nominal V_{OC} of 0.66V compared to H-TiO_2. As seen from the data, the H-HfO_2/TiO_2-based DSSC exhibits an enhanced photoconversion efficiency of 8.6%, whereas H-TiO_2 and P25 TiO_2 show 5.9% and 5.2% efficiency under similar conditions.

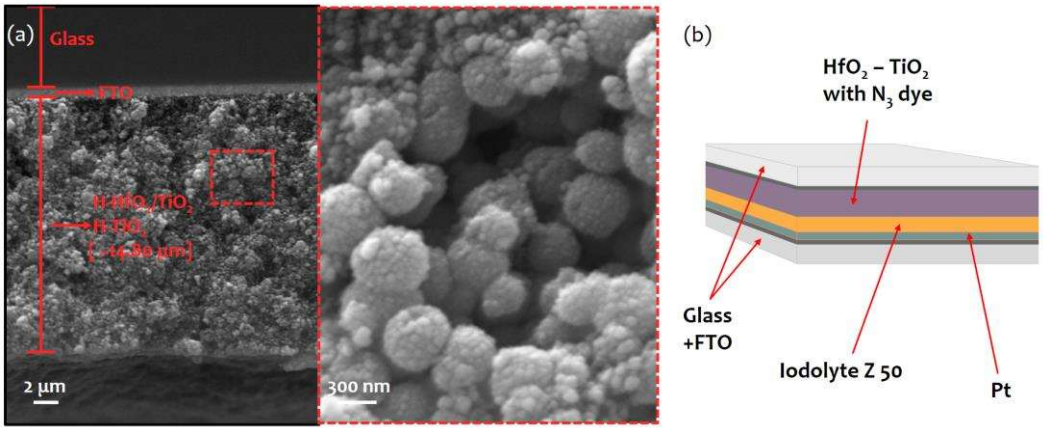

Figure 4.14 : (a) Cross-sectional SEM image of the photoanode deposited on FTO along with its magnified image. Note that Au/Pd metal layer is sputtered on photoanode for improving the image contrast and (b) A schematic showing sandwich model of the fabricated DSSC device

This is an intriguing result and probably occurs due to the enhanced light absorption (discussed in Figure 3.19), higher surface area (Figure 4.15b), and lower recombination rate. From the BET measurements in Figure 4.15b the surface area of H-HfO_2/TiO_2 was calculated to be higher (74.21 m^2g^{-1}) compared to H-TiO_2 (56.186 m^2g^{-1}).

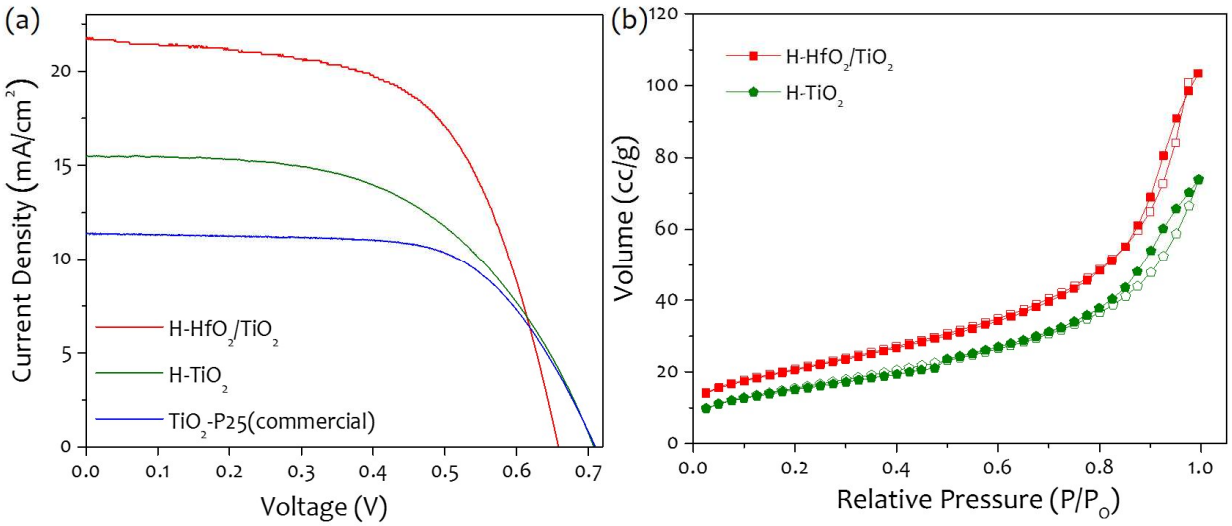

Figure 4.15 : (a) Current density and voltage characteristics of the DSSC fabricated in this study and (b) Nitrogen adsorption-desorption isotherms of H-HfO_2/TiO_2 and H-TiO_2. The isotherm can be classified as type-IV with a hysteresis loop. The surface area of H-HfO_2/TiO_2 is (74.21m^2/g) more as compared to H-TiO_2 (56.186 m^2/g)

The surface area effect was studied by calculating the amount of dye loaded on the photoanode and deloading it using a NaOH solution. The H-HfO_2/TiO_2 photoanode relatively soaked 35% more dye than H-TiO_2. This shows that H-HfO_2/TiO_2 offers a higher surface area thus contributing to the increased efficiency. The absorbance diagram is given in Figure 4.16 along with the detailed calculation given below.

Table 4.8: Photovoltaic performance parameters of the DSSC device fabricated from HfO_2-TiO_2 and TiO_2

Cell	J_{sc} *(mA/cm²)*	V_{oc} *(V)*	*FF*	*η (%)*
H-HfO_2/TiO_2	21.74±0.4	0.66±0.1	60.2±0.08	8.6±0.1
H-TiO_2	15.49±0.1	0.71±0.04	53.97±0.07	5.9±0.9
TiO_2- P25	11.40±0.01	0.71±0.01	64.6±0.01	5.2±0.08

4.3.2 Dye loading

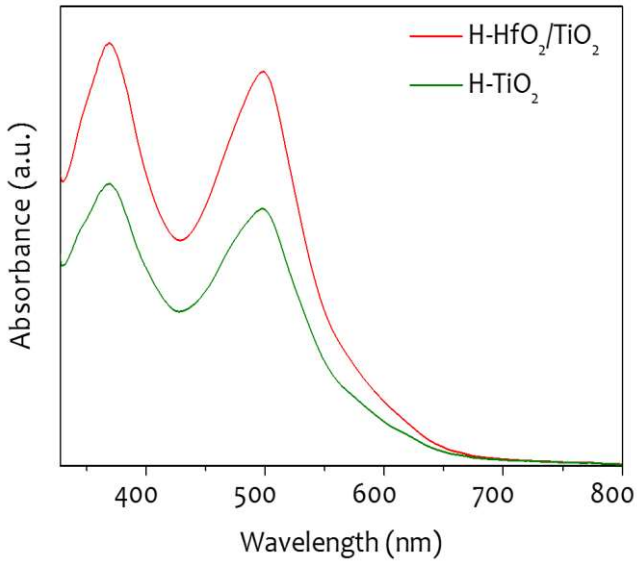

Figure 4.16 : Absorbance spectra of the dye deloaded from H-HfO_2/TiO_2 and H-TiO_2 photoanode

Calculation for dye loading capacity

Concentration of dye absorbed

1. H-HfO_2/TiO_2 = 10.1 × 10^{-9} mol cm^{-2}
2. H-TiO_2 = 6.55 × 10^{-9} mol cm^{-2}

Molar extinction coefficient (ε) for N3 dye at 500 nm is 1.45 × 104 cm^{-1}.

From Beer Lambert's law,

$$A = \varepsilon l c \quad (4.1)$$

where *l* and c are the *length of the cuvette* (1 cm) and *concentration of the dye* respectively.

For H-HfO_2/TiO_2, A = 0.147 (found from the graph)

Thus, concentration of dye absorbed = 1.01 × 10^{-5} M or 10.1 × 10^{-9} mol cm^{-2}

For H-TiO_2, A = 0.095 (found from the graph)

Thus, Concentration of dye absorbed = 6.55 × 10^{-6} M or 6.55 × 10^{-9} mol cm^{-2}

4.3.3 Electron lifetime and charge transfer

Electrochemical impedance spectroscopy (EIS) measurements were performed for DSSCs based on H-HfO_2/TiO_2 and $HTiO_2$ in the frequency range between 1 and 105 Hz under 1 sun illumination for understanding the electron recombination and interfacial charge transfer processes. The Nyquist plots in Figure 4.17a show three semicircles in the complex plane that represent the interface resistance between the photoanode and electrolyte. The plots were fitted to an equivalent circuit consisting of a series resistance (R_S), Pt–electrolyte capacitance, a charge transfer resistance in the counter electrode and the electrolyte interface (R_1 and R_2) and a Warburg resistance, W, due to ion transfer in the electrolyte [Li, Jiao, Xie and Li, 2015]. The parameters, R_S, R_1, R_2, and W, are listed in Table 4.9.

The impedance Bode phase plots in Figure 4.17b display a *frequency peak* (ω_{max}) that corresponds to various charge transfer processes occurring in DSSCs. The Bode plot for H-TiO_2 ω_{max} shifted from 29.10 Hz to 19.54 Hz due to the hydrogenation of HfO_2 in H-HfO_2/TiO_2. The ω_{max} is inversely related to the electron lifetime ($\tau_n = 1/\omega_{max}$). A decrease in the value of u max in DSSC based on H-HfO_2/TiO_2 indicates a decrease in charge recombination compared to $HTiO_2$. The electron lifetime τ_n was calculated using the formula, s τ_n = (R1 × C1), where R1 and C1 are the *charge transfer resistance* and *chemical capacitance* [Lim, Pandikumar, Lim, Ramaraj and Huang, 2015].

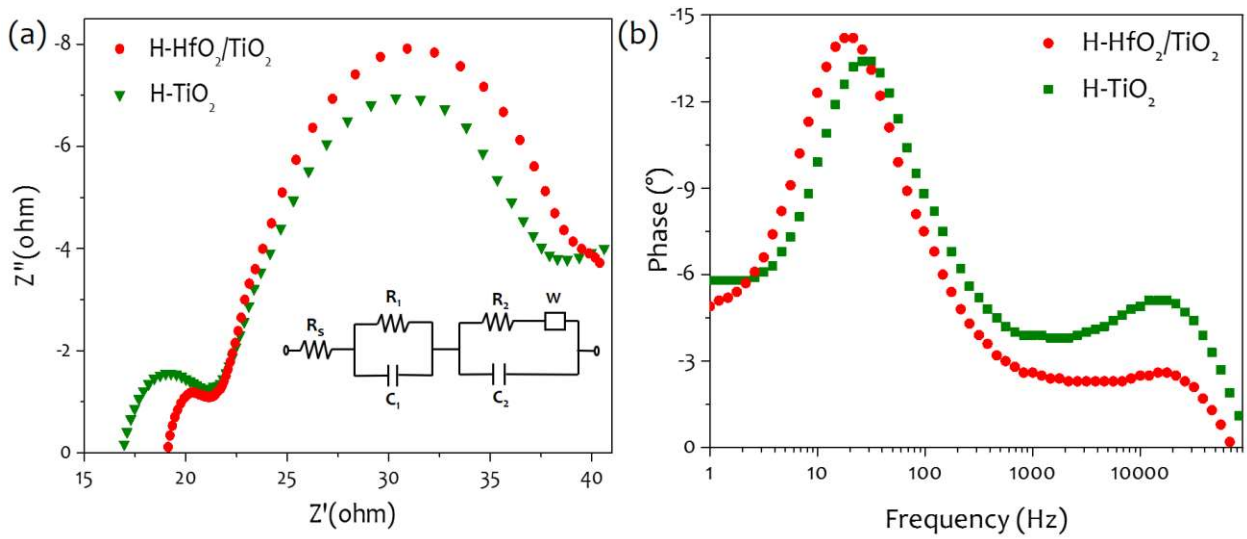

Figure 4.17 : (a) Nyquist plot and (b) Bode plot for the DSSC based on H-HfO_2/TiO_2 and H-TiO_2. Inset of (a) is the equivalent circuit diagram used for fitting the curves

H-HfO_2/TiO_2 was found to have higher τ_n value (0.142 ms) than H-TiO_2 (0.056 ms). This is a significant increase in the electron lifetime, which leads to a reduction in charge recombination in the fabricated device. Thus, a longer electron lifetime (τ_n) and high R_1 value for the H-HfO_2/TiO_2 based DSSC result in improved J_{SC} values.

Table 4.9: EIS performance results of the DSSC device fabricated from H-HfO_2-TiO_2 and H-TiO_2 with R_s (series resistance), R_1 (charge transfer resistance), C_1 (chemical capacitance), τ_n (electron lifetime), and η_c (charge collection efficiency) as the cell parameters

DSSC Sample	R_s (Ω)	R_1 (Ω)	C_1 (μF)	f_{max} (Hz)	$\tau_n=(R_1*C_1)$ (ms)	η_c (%)
H-HfO_2/TiO_2	19.63	14.35	9.898	19.54	0.142	42.23
H-TiO_2	17.5	13.3	4.247	29.10	0.056	43.18

The effect of different HfO_2 loadings and optimization of the hydrogenation conditions will be carried out in future studies for further improving the performance of these devices.

4.4 CONCLUDING REMARKS

Remarkable enhancement in photoconversion efficiency demonstrates the TiO_2 prepared at sub-zero temperature increases charge transport with a decrease in recombination rate at electrolyte–dye–photoanode, a high percentage of anatase phase and harvest more light with different size and shape nanoparticles structure. As excellent photoanode material, ZnO-TiO_2 solid nanosphere emerged as good light-scattering photoanode material due to spherical architecture which provides surface area for electron trapping. Hydrogenated TiO_2 doped with HfO_2 nanodots were reported to increase the defect density upon hydrogenation. The increment in optical adsorption due to band tailoring increases dye uptake capability and exhibited high photoconversion efficiency.